EUROPEAN ORGANIZATION FOR NUCLEAR RESEARCH

Neutron emission in ultraperipheral Pb–Pb collisions at $\sqrt{s_{\mathrm{NN}}} = 5.02$ TeV

ALICE Collaboration

Abstract

In ultraperipheral collisions (UPCs) of relativistic nuclei without overlap of nuclear densities, the two nuclei are excited by the Lorentz-contracted Coulomb fields of their collision partners. In these UPCs, the typical nuclear excitation energy is below a few tens of MeV, and a small number of nucleons are emitted in electromagnetic dissociation (EMD) of primary nuclei, in contrast to complete nuclear fragmentation in hadronic interactions. The cross sections of emission of given numbers of neutrons in UPCs of ^{208}Pb nuclei at $\sqrt{s_{\mathrm{NN}}} = 5.02$ TeV were measured with the neutron zero degree calorimeters (ZDCs) of the ALICE detector at the LHC, exploiting a similar technique to that used in previous studies performed at $\sqrt{s_{\mathrm{NN}}} = 2.76$ TeV. In addition, the cross sections for the exclusive emission of 1, 2, 3, 4 and 5 forward neutrons in the EMD, not accompanied by the emission of forward protons, and thus mostly corresponding to the production of ^{207,206,205,204,203}Pb, respectively, were measured for the first time. The predictions from the available models describe the measured cross sections well. These cross sections can be used for evaluating the impact of secondary nuclei on the LHC components, in particular, on superconducting magnets, and also provide useful input for the design of the Future Circular Collider (FCC-hh).

1   Introduction

Studies of collisions of ultrarelativistic nuclei typically focus on the participant zone where the nuclei overlap and the quark–gluon plasma (QGP), a state of matter where quarks and gluons are free, can be created [1]. This is the domain where hot and dense matter is produced due to the enormous collision energy of the participating nucleons. At the same time, a domain of cold nuclear matter is expected to coexist with the participant zone in peripheral collisions. It is represented by spectator nucleons, which mainly preserve the velocity of the initial nuclei and travel forward. Measurements at the CERN Super Proton Synchrotron (SPS) [2] have shown that some of the spectator nucleons remain bound in nuclear fragments produced in peripheral collisions of ultrarelativistic ^{208}Pb nuclei with a beam energy of 158 GeV per nucleon with a lead target. At this energy heavy spectator fragments were also detected in interactions of ^{208}Pb nuclei with various target nuclei [3]. This was explained by a modest excitation of spectator matter in peripheral collisions [3].

In ultraperipheral collisions (UPCs) of relativistic heavy ions without nuclear overlap the colliding nuclei can be considered entirely as spectators. While their geometrical overlap is excluded because the collision impact parameter exceeds the sum of the nuclear radii, nuclei are still excited by the Lorentz-contracted Coulomb fields of their collision partners. In comparison to hadronic nucleus–nucleus collisions, electromagnetic excitation is a rather soft process that results in the electromagnetic dissociation (EMD) of primary nuclei with the emission of just a few nucleons [4].

Large EMD cross sections for the emission of one, two and three forward neutrons have been reported by the ALICE collaboration [5] for UPCs of ^{208}Pb nuclei at a centre-of-mass energy per nucleon pair $\sqrt{s_{NN}} = 2.76$ TeV at the Large Hadron Collider (LHC). EMD products retain beam rapidity similarly to spectators from hadronic nucleus–nucleus collisions. The EMD of ^{208}Pb nuclei contributes significantly to the decay of the beam intensity [6] and produces various secondary nuclei in all four interaction points (ALICE, ATLAS, CMS and LHCb) of the LHC [7]. Certain secondary nuclei with their charge-to-mass ratio close to ^{208}Pb (principally ^{207}Pb) can travel for long distances around the collider rings because their magnetic rigidity is close to that of ^{208}Pb and they may potentially be lost in superconducting magnets [7, 8]. With a proper set-up of the collimation system, most of these secondary nuclei are intercepted efficiently by the off-momentum collimators and the dispersion suppressor sections around the LHC experiments. A dominant source of beam loss in the latter regions is the process of bound-free e^+e^- pair production in UPCs with the electron capture by ^{208}Pb [7, 8].

The methods to study fragmentation of projectile nuclei at multi-GeV or TeV collision energies differ significantly from those used at much lower collision energies. In the latter case, fragments of projectiles with an initial energy of hundreds of MeV per nucleon are emitted at large angles with respect to the beam axis, so that their spread permits complete identification of projectile fragments using, among others, scintillator hodoscopes and time-of-flight detectors [9, 10]. In particular, the multi-fragment break-up of spectator matter has been investigated at intermediate collision energies [9].

In contrast, the detection of projectile fragments in experiments at ultrarelativistic energies exceeding tens of GeV per nucleon is harder. It is difficult to separate these fragments from beam nuclei because they are emitted at very small angles with respect to the beam axis. For example, projectile fragments were intercepted by imposing an external magnetic field and placing fragment detectors far from the interaction point [2]. High resolution nuclear emulsions [11] and solid-state track detectors made of CR39 plastic [12] have also been employed to study fragmentation of ultrarelativistic nuclei. The charge distributions of fragments have been measured [11, 12] in a wide range of charges of secondary nuclei, but nuclear emulsions and stacks of CR39 remained insensitive to spectator neutrons. Measurements of the charge-changing cross sections for lead and indium nuclei at an energy of 158 GeV per nucleon were performed with multiple-sampling ionisation chambers in Refs. [3] and [13], respectively, also without detecting forward neutrons.

It should be emphasised that, to date, the production of charged spectator fragments has not been studied neither at RHIC nor at the LHC. There exist only two proposals for future experiments to detect charged fragments in collider experiments, in particular, by means of a centrality detector at RHIC [14] and by the ATLAS Forward Proton detectors at the LHC [15]. The ALICE experiment already has a unique possibility to detect forward protons as well as neutrons with its neutron and proton zero degree calorimeters (ZDCs) [16–18].

According to the RELDIS [4, 19, 20] and FLUKA [21] models, the production of various secondary nuclei is expected in EMD of ^{208}Pb at the LHC. It is impossible to identify masses and charges of secondary nuclei at the LHC and thus directly measure the cross sections of production of specific nuclides. However, the cross sections of production of ^{207,206,205,204,203}Pb are closely related to the cross sections to emit 1, 2, ... 5 neutrons, respectively, in the absence of proton emission.

The aim of the present work is twofold. Firstly, to determine the cross sections of neutron emission in EMD of heavy nuclei at the highest collision energy available in accelerator experiments. Various models [4, 21–23] that are used to calculate neutron emission in EMD can be tested with these new data. Secondly, to measure the cross sections of emission of 1, 2, ... 5 neutrons without protons, to be used as approximations of the cross sections of production of ^{207,206,205,204,203}Pb. The validity of this approximation is studied by means of the RELDIS model.

In Section 2 the ALICE ZDCs are briefly described. In Section 3 the data sample and the adopted trigger configuration are presented. Section 4 describes the methods of fitting ZDC energy spectra, and the corrections for detection efficiency and acceptance that provided the measured cross sections presented in Section 5. In Section 6, on the basis of the RELDIS model, the neutron emission without protons in EMD of ^{208}Pb is associated with the production of secondary lead nuclei. Finally, conclusions and outlook are given in Section 7.

2   Experimental set-up

A detailed description of the ALICE experiment can be found in Ref. [24]. In the following, only the detectors relevant for the measurements discussed in this paper will be described. Two identical systems of hadronic calorimeters are placed on both sides (C and A) of the nominal interaction point (IP), 112.5 m away from the IP along the beam direction. The neutron (ZNC and ZNA) and proton (ZPC and ZPA) calorimeters [16–18] were denoted as ZN and ZP, respectively. The letter C(A) was assigned to the corresponding calorimeter because it intercepts the forward nucleons emitted by nuclei of the clockwise (anticlockwise) beam 1(2). Each ZDC is segmented into four towers. Half the optical fibres uniformly distributed in the calorimeter are read out by four tower photomultipliers (PMTs) and the other half are read out by a single fifth photomultiplier (PMC) common to all towers. Thus, there exist two options to obtain the energy deposited in the ZDC, either from the sum of signals in all PMTs (including PMC), or from the signal in the PMC alone.

ZNC and ZNA are placed at zero degrees with respect to the neutron flight path from the IP to detect neutral forward particles at pseudorapidities $|\eta| > 8.8$. ZPC and ZPA detect forward protons guided to these calorimeters by the LHC magnet system. Two small electromagnetic calorimeters (ZEM1 and ZEM2) are placed only on the side A, at 7.5 m from the IP, covering the pseudorapidity range $4.8 \leq \eta \leq 5.7$ [18] and two intervals $-16° < \phi < 16°$ and $164° < \phi < 196°$ of azimuthal angle.

3   Data sample

Data on ^{208}Pb–^{208}Pb collisions at $\sqrt{s_{NN}} = 5.02$ TeV collected by ALICE in 2018 were analysed. Special runs for the EMD cross section measurement with reduced instantaneous luminosity and, consequently, with reduced event pile-up were considered. For these runs the average number of hadronic inelastic

3

interactions per bunch crossing $\mu_{inel} \sim 1.3 \times 10^{-4}$ was about 10 times lower than during the ALICE standard physics runs. Events were triggered requiring a signal over threshold either in ZNC or in ZNA. This condition is referred to as the ZED trigger and it is sensitive to one-sided EMD events with neutrons emitted either towards the C or A sides, as well as to EMD and hadronic events with neutrons emitted on both sides. It is customary (see, e.g. [5]) to define as single EMD events those with at least one neutron emitted in EMD processes, and as mutual EMD events those with at least one neutron emitted per side in EMD processes, so that mutual EMD events are a subset of single EMD events.

Using the ZDC timing information, only events corresponding to interactions happening at the nominal bunch crossing were selected, thus rejecting collisions between the beam and residual gas in the beam pipe, and collisions involving nuclei circulating outside the nominal bunch slots. The total number of selected events amounts to $N_{tot} = 2.050 \times 10^6$. The ZED trigger cross section σ_{ZED} was measured in a van der Meer (vdM) scan [25] and found to be $\sigma_{ZED} = 420.5 \pm 9.3$ b [26].

The triggered events were classified into electromagnetic and hadronic events according to the signals of the forward calorimeters ZEM1 and ZEM2. Events with a signal in either ZEM were tagged as hadronic and rejected, leaving a sample of $N^{EMD}_{tot} = 2.009 \times 10^6$ single or mutual EMD event candidates. However, as follows from the modelling of particle emission in UPCs of ^{208}Pb at the LHC [19], in a small fraction of EMD events, protons and pions are emitted at $|\eta| \leq 6$. Detection of these particles by one of the ZEMs may lead to the rejection of EMD events due to the ZEM veto condition. Therefore, it is necessary to estimate the efficiency of the ZEM veto to select electromagnetic events.

Let the numbers of single EMD, mutual EMD and hadronic events be denoted as s, m and h, respectively. The number of detected events with neutrons, say, only on side C is defined as $s - m + h\zeta_{hnm} = \mathcal{N}_1$. In this equation a small fraction ζ_{hnm} of hadronic non-mutual events with the emission of forward neutrons only on one side is taken into account. The number of events with neutrons only on side C, but obtained without signal in ZEM is calculated as $s\varepsilon - m\varepsilon_m + h\zeta_{hnm}\varepsilon_h = \mathcal{N}_2$. Here the fractions of single EMD, mutual EMD, and hadronic events, which survive the ZEM veto, are denoted as ε, ε_m, and ε_h, respectively. The condition that neutrons are detected only on side C can be released, thus providing the equations: $s + h = \mathcal{N}_3$ and $s\varepsilon + h\varepsilon_h = \mathcal{N}_4$, without and with the ZEM veto, respectively. In Ref. [5] a small value $\varepsilon_h = 0.076$ was reported on the basis of HIJING modelling. According to the AAMCC model [27], the fraction of hadronic events with 1–5 forward neutrons on a given side, but without neutrons on the other side, is calculated as $\zeta_{hnm} = 0.003$. As estimated with the RELDIS and AAMCC models, for each of the 1n–5n channels, the relation $s \gg h$ is valid, and consequently, $s \gg h\varepsilon_h$. Because of the dominance of single EMD events over mutual EMD events, the relations $s - m \gg h\zeta_{hnm}$ and $s\varepsilon - m\varepsilon_m \gg h\zeta_{hnm}$ are also valid and the hadronic contribution can be neglected in all four equations for each neutron multiplicity with the solution $\varepsilon = \mathcal{N}_4/\mathcal{N}_3$ and $\varepsilon_m = (\mathcal{N}_4 - \mathcal{N}_2)/(\mathcal{N}_3 - \mathcal{N}_1)$.

The resulting ε_i for each neutron multiplicity $i = 1, 2, \ldots 5$ for events with less than 6 neutrons and for events with any number of neutrons (Xn) are given in Table 1 together with their uncertainties calculated following Ref. [28]. The values of ε_i estimated on both sides exceed 99%. As can be also seen from Table 1, there is a trend that the higher the neutron multiplicity, the higher the fraction of EMD events lost due to the ZEM veto. Hereafter, events with zero, one, two, ... six neutrons are denoted as 0n, 1n, 2n, ... 6n events. Less than 0.125% of 1n events are lost due to the ZEM veto, but up to 1% for 5n. This is explained by the fact that EMD products associated with high neutron multiplicity events are emitted at larger angles and in some rare cases can hit ZEM. Nevertheless, the efficiency of selecting EMD events by imposing the ZEM veto remains extremely high ($> 99.8\%$) for the 1n–5n channels. The values of ε_i listed in Table 1 were used to correct the numbers of detected events n_i, of each neutron multiplicity in, for the efficiency of the ZEM veto to select EMD events.

The emission of neutrons in the EMD of one or both colliding nuclei can be accompanied by two-photon interactions $\gamma\gamma \to e^+e^-$ in the same UPC event. This process was considered in Ref. [29] for mutual

Table 1: Efficiency of the ZEM veto to select electromagnetic events with a given neutron multiplicity and for events with any number of neutrons, estimated from the data collected with and without the ZEM veto for the sides C and A.

Neutron multiplicity in	ε_i (%)	
	Side C	Side A
1n	99.875 ± 0.005	99.902 ± 0.005
2n	99.766 ± 0.014	99.819 ± 0.013
3n	99.457 ± 0.039	99.349 ± 0.042
4n	99.479 ± 0.043	99.321 ± 0.049
5n	99.368 ± 0.050	99.025 ± 0.064
total 1n–5n	99.802 ± 0.005	99.806 ± 0.005
total Xn	96.722 ± 0.017	96.117 ± 0.019

EMD. By modelling with STARlight [30] dilepton production and neutron emission on one side, the energy distributions of e^+ and e^- within the acceptance of the ZEM were calculated. The probability to obtain leptons with energy above the ZEM veto threshold of about 10 GeV was found to be negligible.

4   Analysis

4.1   Collection, calibration and fit of ZDC energy spectra

In the present work the ZDC energy spectra collected with the PMC were used to obtain the neutron emission cross sections. These spectra were calibrated to satisfy as precisely as possible two main criteria: (1) the pedestal peak is centred at zero energy; (2) the distance between consecutive peaks amounts to the beam energy $E_0 = 2510$ GeV per nucleon.

The numbers of detected events n_i for each neutron multiplicity class in were extracted by fitting the calibrated distributions of energy E deposited in ZN using the χ^2 fit method. The fitting procedures were validated with Run 1 data in Ref. [5]. The fitting function $F(E)$ is the sum of six Gaussians corresponding to up to six detected neutrons

$$F(E) = \sum_{i=1}^{6} G_i(E) = \sum_{i=1}^{6} \frac{n_i}{\sqrt{2\pi}\sigma_i} \, \mathrm{e}^{-\frac{(E-\mu_i)^2}{2\sigma_i^2}} \, . \tag{1}$$

The Gaussian $G_i(E)$ represents the i-th peak and it is characterised by the mean value μ_i, the standard deviation σ_i and the normalisation constant n_i, which denotes the number of detected events with i neutrons. Because of the large widths of the peaks corresponding to neutron multiplicities larger than 5 in the neutron spectra, it was not possible to identify unambiguously the numbers of events with six or more neutrons. Though the 6n peak is not well-defined, it is still used to improve fit results for 1, 2, ... 5 neutrons. The values of μ_1, σ_1 and n_1 for the first nucleon peak were considered as free parameters. Despite the expected exact correspondence of μ_1 to E_0, some variations of μ_1 in the course of the fitting procedure were allowed within a $\pm 10\%$ deviation from E_0. In addition, the value of σ_1 was constrained to be between $0.1 \times E_0$ and $0.5 \times E_0$ to improve the fit quality. These conditions make it possible to account for imperfect ZDC calibration. The parameters of the Gaussians describing the two-, three-, four-, five- and six-nucleon peaks were also restricted: μ_i varied within $\pm 20\%$ around $i \times \mu_1$ while σ_i varied from σ_1 to $\sqrt{i}\sigma_1$. The numbers of detected events n_i in each peak were introduced as free parameters of the fit. As described below, after taking into account the acceptance$\times$efficiency of the ZDCs, corrected numbers of events N_i were finally obtained from n_i.
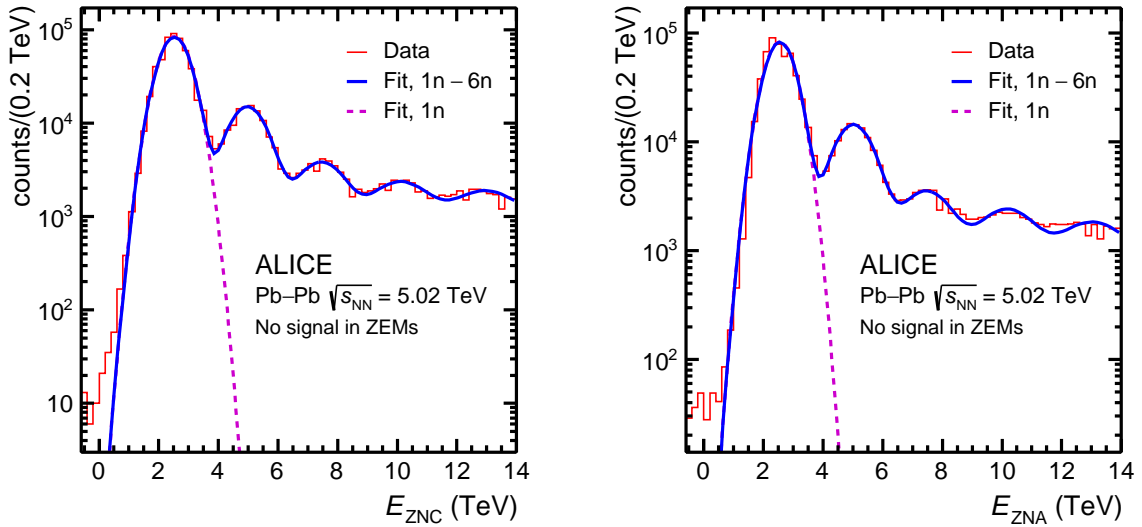
Figure 1: Colour online: distributions of energy in ZNC (left) and ZNA (right) from EMD events (histograms) and resulting fit functions (solid curves) representing the sum of Gaussians. The Gaussians representing 1n peaks are shown by dashed curves.

The distributions of energy deposited by forward EMD neutrons in ZNC and ZNA are shown in Fig. 1. These distributions were obtained for events with at least one neutron registered either in ZNC (Fig. 1, left) or in ZNA (Fig. 1, right), surviving the ZEM veto. As seen from this figure, the spectra collected on the C and A sides are very similar. These spectra were fitted with the functions given by Eq. (1). The yields of 1n, 2n, ... 5n EMD events were extracted from these spectra and used to calculate the cross section of emission of given numbers of neutrons along with any number of forward protons, as described in Section 5.1.

4.2 Correction for detection efficiency and acceptance of neutron and proton ZDCs

Some of the forward nucleons are lost on their way to the ZDCs due to the limited ZDC acceptance and scattering on various components of the LHC, in particular, on injection collimators, beam pipes, recombination chamber and in air. Also, a peripheral impact of some nucleons on the calorimeter is responsible for an increased shower leakage leading to reduced energy deposited in the ZDCs. Because of such effects, the distributions of energy deposited in the ZDCs are distorted, particularly in events with a high nucleon multiplicity. For example, either one or two nucleons can be lost in a three-nucleon event. As a result, the three-nucleon event can be misidentified, respectively, as a two-nucleon or as a one-nucleon event. The probability to obtain a fake one-nucleon event will be different in two- and three-nucleon events. This suggests the need to calculate the efficiency of event detection separately for each multiplicity class, as demonstrated in Ref. [31].

The acceptance×efficiency correction factors $f_{in} = N_i^{MC}/n_i^{MC}$ were calculated for ZNC and ZNA and, for the study of neutron emission without protons, also for ZPC and ZPA. In a realistic Monte Carlo simulation of the ALICE apparatus, and after transporting neutrons generated with RELDIS, the number of generated events N_i^{MC} and the number of events n_i^{MC} registered in ZDC were calculated for each neutron multiplicity class in. RELDIS has been validated with data on neutron emission in EMD of ^{208}Pb at the LHC [5] and at lower collision energies [32]. The acceptance×efficiency correction factors calculated for the channels with the emission of 0, 1, 2, ... 5 neutrons, possibly along with other particles, are given in Table 2. The values of f_{in} were obtained by two different methods described below, and the simple averages f_{in} were applied to raw data, as explained in Section 4.3. The first method was based

6

Table 2: Acceptance×efficiency correction factors for detecting neutrons in ZNC and ZNA and their estimated uncertainties.

Neutron multiplicity in	Average of two methods f_{in}	
	ZNC	ZNA
0n	0.286 ± 0.126	0.302 ± 0.097
1n	1.064 ± 0.031	1.064 ± 0.030
2n	1.092 ± 0.024	1.010 ± 0.095
3n	1.057 ± 0.032	1.066 ± 0.020
4n	1.001 ± 0.046	0.962 ± 0.094
5n	0.907 ± 0.132	0.917 ± 0.104

on counting nucleons crossing the front area of each ZDC, while in the second method simulated ZDC energy spectra were fitted by the functions given by Eq. (1). Finally, in both methods the numbers of events of each multiplicity in generated by RELDIS were divided by the numbers of detected events to obtain the correction factors. The difference between the results of the two methods divided by $\sqrt{2}$ is considered as the systematic uncertainty for the final average correction factors. These factors are given in Table 2 together with their combined statistical and systematic uncertainties. As seen from this table, most of the obtained f_{in} values exceed unity, because the loss of EMD neutrons in a channel of a certain multiplicity is not compensated by the migration of events from less frequent channels of higher multiplicity induced by the loss of one or two neutrons. In contrast, according to RELDIS, only in 3.2% of EMD events neutrons are not emitted, but the 0n channel is filled with events of different neutron multiplicity when all neutrons are lost. This explains a noticeable correction of $f_{0n} \sim 0.3$ for the 0n channel.

When considering neutron emission without associated proton emission, additional correction factors for the proton ZDC, f_{0p}, were applied to the raw yields. Hereafter, events with zero protons are denoted as 0p events. These correction factors were calculated with the same two methods as for the neutron ZDC resulting in the average values of 0.848 ± 0.015 and 0.852 ± 0.018 for ZPC and ZPA, respectively. In general, results from MC simulations are consistent with results of the probabilistic model of Ref. [31] with the probability $p_n = 0.9$ to detect a neutron in ZN and with $p_p = 0.55$ to detect a proton in ZP.

4.3 Determination of neutron emission cross sections

The cross sections for specific EMD channels $\sigma(in)$ with a given number of neutrons i and an arbitrary number of protons were obtained by combining σ_{ZED} introduced in Section 3 and n_i from the fit functions given by Eq. (1). The cross sections were measured separately on the C and A sides by ZNC and ZNA, respectively. After the signal extraction, the corrections for the efficiency of the ZEM veto ε_i introduced in Section 4.1 and for the ZDC efficiency and acceptance, f_{in}, Section 4.2, were applied:

$$\sigma(in) = \sigma_{ZED}\frac{N_i}{N_{tot}} = \sigma_{ZED}\frac{n_i}{N_{tot}}\frac{f_{in}}{\varepsilon_i} = \sigma_{ZED}\frac{n_i}{N_{tot}}F_{in} \ . \tag{2}$$

Here N_i is a corrected number of events with given neutron multiplicity i, N_{tot} is the total number of ZED trigger events defined in Section 3, and F_{in} is the resulting correction factor. The cross sections of specific EMD channels $\sigma(in, 0p)$ with given number of neutrons i and without protons on the side C or A were obtained in the same way, but with the additional correction factors f_{0p} for the efficiency of registration of 0p events in ZPC and ZPA, respectively:

$$\sigma(in, 0p) = \sigma_{ZED}\frac{N_i}{N_{tot}} = \sigma_{ZED}\frac{n_i}{N_{tot}}\frac{f_{in}f_{0p}}{\varepsilon_i} = \sigma_{ZED}\frac{n_i}{N_{tot}}F_{in,0p} \ . \tag{3}$$

Table 3: Relative systematic uncertainties of the cross sections of emission of given numbers of neutrons *i* accompanied by an arbitrary number of protons (Yp, including zero protons) and without protons (0p), in UPCs of ^{208}Pb nuclei at $\sqrt{s_{NN}} = 5.02$ TeV. Each uncertainty is calculated for the average of the cross sections measured on the sides C and A.

Source	Relative uncertainty (%)									
	1n		2n		3n		4n		5n	
	Yp	0p	Yp	0p	Yp	0p	Yp	0p	Yp	0p
Fitting procedure	0.55	0.55	0.32	0.29	0.83	0.72	0.73	0.67	1.14	1.01
ZDC+ZEM efficiency	2.03	2.45	4.68	4.88	1.78	2.25	5.35	5.52	9.26	9.36
σ_{ZED} determination from vdM scan	2.2									
Total	3.04	3.34	5.18	5.36	2.95	3.23	5.83	5.98	9.59	9.67

Here $F_{in,0p}$ is the resulting correction factor as in Eq. (2), but for 0p events. Because of the very large number of collected ZED trigger events, the uncertainty of N_{tot} is negligible. The statistical uncertainties of n_i originate from the uncertainties on the numbers of events found by the fit procedure. The systematic uncertainties of n_i were estimated from a variation of the fit procedure by considering the difference in n_i obtained with the nominal and double bin size. Only systematic uncertainties were considered for F_{in} and $F_{in,0p}$. Following Ref. [26], the relative systematic uncertainty of σ_{ZED} was taken as 2.2%, resulting from the vdM scan analysis.

The final cross sections were obtained as the average between the measurements performed on the sides C and A from the event numbers and resulting correction factors introduced in Eqs. (2) and (3):

$$\bar{\sigma} = \frac{\sigma^{C} + \sigma^{A}}{2} = \sigma_{\text{ZED}} \frac{n^{C}F^{C} + n^{A}F^{A}}{2N_{\text{tot}}} \quad . \tag{4}$$

The contributions to the relative systematic uncertainties of $\bar{\sigma}$ were propagated from the systematic uncertainties on each side as summarised in Table 3. These uncertainties were calculated separately for the cross sections of neutron emission accompanied by an arbitrary number of protons (Yp, including zero protons) and without proton emission (0p).

In these measurements, the pile-up of EMD events was lower with respect to the previous ALICE measurements of the EMD cross sections [5]. Nevertheless, the uncertainty due to the residual pile-up of EMD events was also addressed. The main issue with the pile-up is to count two 1n events as a 2n event. For these runs the average number of hadronic inelastic interactions per bunch crossing μ_{inel} was about 1.3×10^{-4}. The same value, but calculated for 1n emission in EMD is $\mu_{1n} = \mu_{\text{inel}} \times (\sigma_{1n}/\sigma_{\text{had}}) = 1.8 \times 10^{-3}$, where $\sigma_{1n} = 108$ b is calculated with RELDIS and $\sigma_{\text{had}} = 7.67 \pm 0.24$ b is the inelastic hadronic interaction cross section measured in Ref. [26]. With $\sigma_{2n}/\sigma_{1n} \approx 0.24$, also estimated with RELDIS, the relation $\mu_{2n} \approx 0.24 \times \mu_{1n}$ is obtained. Following the Poisson distribution, the ratio of the probabilities to obtain two 1n events in the same bunch crossing $p(2, \mu_{1n})$ and to have one 2n event $p(1, \mu_{2n})$ is

$$\frac{p(2, \mu_{1n})}{p(1, \mu_{2n})} = \frac{\mu_{1n}^2 \exp(-\mu_{1n})}{2\mu_{2n} \exp(-\mu_{2n})} = \frac{\mu_{1n}}{0.48} \exp(-0.76\mu_{1n}) \approx 0.004 \quad . \tag{5}$$

One can conclude that the pile-up effect of 0.4% for 2n emission can be neglected in view of the total $\sim 5\%$ uncertainty for this channel reported in Table 3.

5 Results

5.1 Cross sections of emission of given numbers of neutrons

The EMD cross sections $\sigma(in)$ for 1n, 2n, 3n, 4n and 5n emission accompanied by an arbitrary number of forward protons (including zero protons) were measured separately on the C and A sides. They are listed in Table 4. In order to obtain these cross sections, EMD events were selected by applying a veto on ZEM, as described in Section 3. The cross sections given in Table 4 were corrected for the ZDC and ZEM efficiency separately for each side as described in Section 4.2. As seen, the cross sections measured on the side C are slightly larger compared to those on the side A. However, the side C and A cross sections are in most cases consistent, because this difference is within the uncorrelated uncertainty of the side A cross section. As follows from Table 3, the main contribution to the systematic uncertainties of the cross sections is due to the uncertainties of the corrections for ZDC and ZEM efficiency.

The average $\sigma(in)$ between the C and A sides were calculated for each neutron multiplicity i according to Eq. (4). The resulting $\sigma(in)$ are given in Table 4 with their statistical and systematic uncertainties propagated from the uncertainties on each side, which were considered as uncorrelated, except for the contribution from the vdM scan uncertainty, which is fully correlated between the C and A sides. The differences between the cross sections obtained on the sides C and A depend on the chosen method to calculate the ZDC efficiency, with the exception of 1n channel, so the uncertainties on the efficiency can justify the difference between the cross sections on the C and A sides. On the basis of this finding, the difference between C and A sides divided by $\sqrt{2}$ was considered as an additional uncertainty only for the average 1n cross section.

In Table 4 the measured cross sections are compared with results of the RELDIS [4] and n$_O^O$n [23] models. Both models are based on the Weizsäcker–Williams method to calculate the cross sections of neutron emission in EMD of nuclei by considering the respective photonuclear reactions induced by equivalent photons. RELDIS simulates nuclear reactions induced by Weizsäcker–Williams photons on ^{208}Pb by means of the intranuclear cascade model of photonuclear reactions with the subsequent de-excitation of residual nuclei via neutron evaporation and other processes [33]. A phenomenological approximation for the total photoabsorption cross section on ^{208}Pb is used as an input to RELDIS together with calculated relative contributions of various final states to obtain the absolute values of $\sigma(in)$ and $\sigma(in, 0p)$. A similar phenomenological approximation of the total photoabsorption cross section is also used in n$_O^O$n. In this event generator the calculations of probability of a given neutron emission channel are based on approximations of partial photoneutron cross sections measured on ^{208}Pb below 140 MeV and extrapolated to higher photon energies [23]. Only neutron emission events can be generated with n$_O^O$n, but the 0n EMD cross section of 6.85 b corresponding to 3.2% of EMD events with the emission of other particles without neutrons was calculated with RELDIS.

The uncertainties of RELDIS results ($\sim 5\%$) given in Table 4 stem from the uncertainty of the phenomenological approximation of the total photoabsorption cross section on ^{208}Pb used by this model. As shown in Ref. [20], the uncertainties of the calculations of specific neutron emission channels (1n, 2n) in absorption of low energy photons are typically as high as 7%. Another source of uncertainties is connected to the estimations of unknown total nuclear photoabsorption cross section at high photon energies (> 60 GeV) from the measured total γp cross sections taking into account nuclear shadowing. As evaluated recently [34], the total EMD cross sections calculated with different high-energy approximations for ^{208}Pb–^{208}Pb collisions at the LHC differ by $\sim 2\%$. Similar uncertainties of ~ 2–4% were attributed to the measured total cross section of the absorption of real intermediate energy photons (0.5–2.6 GeV) by ^{nat}Pb [35]. The total EMD cross section is the sum of the contributions of processes induced by Weizsäcker–Williams photons from the above-mentioned energy domains. Therefore, the combined error of $\sim 5\%$ is attributed to the cross sections calculated with RELDIS also for each individual neutron emission channel in Table 4. The uncertainty of 2% also applies to the cross sections calculated with n$_O^O$n

Table 4: Cross sections of emission of one, two, three, four and five neutrons along with an arbitrary number of protons in EMD of ^{208}Pb at $\sqrt{s_{NN}} = 5.02$ TeV measured on the C and A sides and their average along with their statistical and systematic uncertainties. Cross sections calculated with RELDIS [4] and n$_O^O$n [23] are given for comparison. The sum of 1n–5n cross sections is presented in the last row. The uncertainties of the measurements are reported in the order $\pm$ (stat.) $\pm$ (syst.).

ZN	$\sigma(in)$ (b)		$\sigma(in)$ (b)	$\sigma^{RELDIS}(in)$ (b)	$\sigma^{n_O^On}(in)$ (b)
	Side C	Side A			
1n	$109.7 \pm 0.1 \pm 4.0$	$107.2 \pm 0.1 \pm 4.0$	$108.4 \pm 0.1 \pm 3.7$	108.0 ± 5.4	103.7 ± 2.1
2n	$25.8 \pm 0.1 \pm 0.8$	$24.1 \pm 0.1 \pm 2.3$	$25.0 \pm 0.1 \pm 1.3$	25.9 ± 1.3	23.6 ± 0.5
3n	$7.97 \pm 0.07 \pm 0.32$	$7.94 \pm 0.04 \pm 0.24$	$7.95 \pm 0.04 \pm 0.23$	11.4 ± 0.6	6.3 ± 0.1
4n	$5.73 \pm 0.04 \pm 0.30$	$5.56 \pm 0.04 \pm 0.56$	$5.65 \pm 0.03 \pm 0.33$	7.8 ± 0.4	4.8 ± 0.1
5n	$4.61 \pm 0.04 \pm 0.68$	$4.47 \pm 0.04 \pm 0.52$	$4.54 \pm 0.03 \pm 0.44$	6.3 ± 0.3	4.7 ± 0.1
1n–5n			$151.5 \pm 0.2 \pm 4.6$	159.8 ± 5.6	143.1 ± 2.2

because of the uncertainties of the approximation of the total photoabsorption cross section on ^{208}Pb.

The sum of the measured 1n–5n cross sections amounts to $151.5 \pm 0.2 \pm 4.6$ b, and it is within 2σ in agreement with the same sum calculated with RELDIS as 159.8 ± 5.6 b, see Table 4. The 1n–5n sum calculated with n$_O^O$n as 143.1 ± 2.2 is lower. In general, the measured sum is in the middle between the models. The total single EMD cross section for neutron emission can be simply estimated from the cross sections measured in Ref. [26] as $(\sigma_{ZED} - \sigma_{had})/2 = 206.4$ b assuming 100% efficiency of the ZED trigger. It is in good agreement with the corresponding cross section of 204.6 ± 7.1 b calculated with RELDIS. As seen, the measurements and calculations demonstrate dominant contributions of 73% and 78%, respectively, of 1n–5n channels to the EMD of ^{208}Pb leading to neutron emission.

The measured cross sections are also shown in Fig. 2 together with results of the models. As seen, the cross sections of 1n- and 2n-emission calculated with RELDIS and n$_O^O$n agree with the measured ones. On the other hand, the measured 3n and 4n cross sections are overestimated by RELDIS and underestimated by n$_O^O$n. At the same time, the 5n cross section is described very well by n$_O^O$n, but overestimated by RELDIS. One can note that the models agree well with respect to the 1n and 2n cross sections, but differ for higher neutron multiplicities. This indicates the importance of 3n, 4n and 5n measurements for tuning the parameters of the models mentioned above.

5.2 Comparison with previous ALICE results

Previous ALICE results on neutron emission in EMD were reported in Ref. [5] for ^{208}Pb–^{208}Pb collisions at $\sqrt{s_{NN}} = 2.76$ TeV. Events were required to have a signal in one of the two ZN and no signal in the other one, so events of symmetric emission, such as those occurring in hadronic and mutual EMD were rejected, and the sample contained single but not mutual EMD events. The ZEM veto was not used to suppress hadronic events. With this selection the fractions of 1n, 2n and 3n events were determined in Ref. [5]. Following the same selection, the spectra in ZNC and ZNA for single minus mutual EMD process were obtained also in the present work at $\sqrt{s_{NN}} = 5.02$ TeV without the ZEM veto described in Section 3.

The fractions of 1n-, 2n-, 3n- and 4n-events over the total number of events without neutrons on the opposite side $N_{one-side}$ are listed in Table 5. These fractions were extracted from ZNC and ZNA spectra and were corrected for ZNC and ZNA acceptance as described in Section 4.2. The measurements are compared with RELDIS results given in the same table. The previous ALICE results for ^{208}Pb–^{208}Pb collisions at $\sqrt{s_{NN}} = 2.76$ TeV [5] are also given together with RELDIS results for this collision energy.
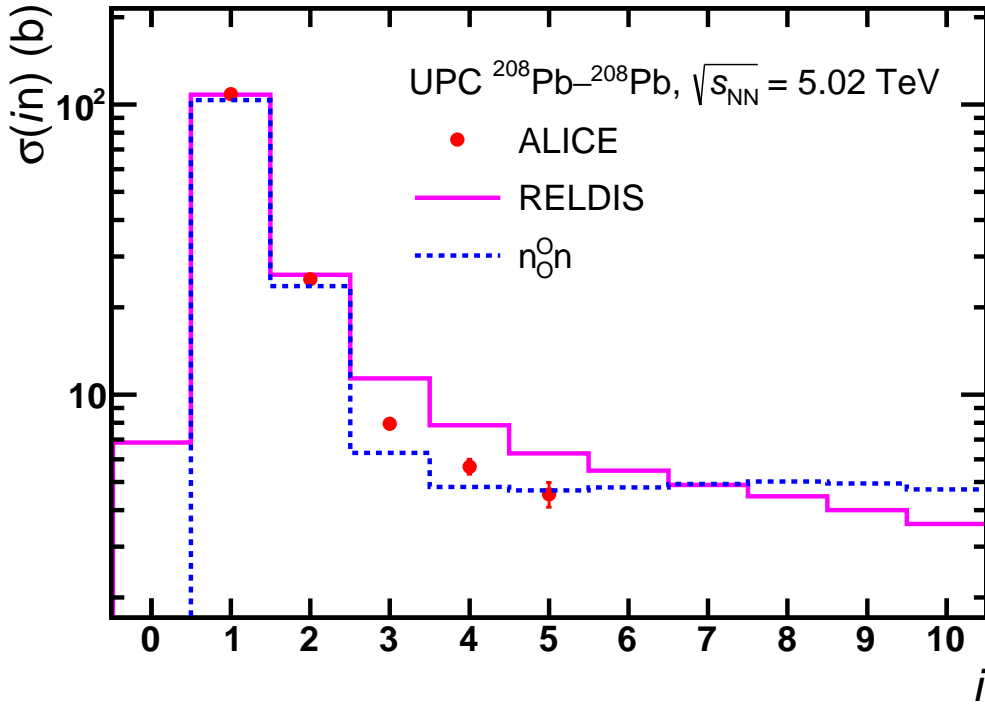
Figure 2: Colour online: measured (points) and calculated with RELDIS [4] (solid-line histogram) and $n_O^O n$ [23] (dashed-line histogram) cross sections of emission of given numbers of neutrons i in UPCs of ^{208}Pb nuclei at $\sqrt{s_{\mathrm{NN}}} = 5.02$ TeV. Combined statistical and systematic uncertainties of the measurements are presented.

Table 5: Fractions (in %) of EMD events with given numbers of neutrons but without neutrons on the opposite side measured and calculated for ^{208}Pb–^{208}Pb UPCs at $\sqrt{s_{\mathrm{NN}}} = 2.76$ TeV [5] and $\sqrt{s_{\mathrm{NN}}} = 5.02$ TeV. The uncertainties of the measurements are given in the order $\pm$ (stat.) $\pm$ (syst.).

| Single minus | $\sqrt{s_{\mathrm{NN}}} = 2.76$ TeV [5] | | $\sqrt{s_{\mathrm{NN}}} = 5.02$ TeV | |
mutual	Experiment	RELDIS	Experiment	RELDIS
$N_1/N_{\mathrm{one\text{-}side}}$	$51.5 \pm 0.4 \pm 0.2$	54.2 ± 2.4	$52.4 \pm 0.1 \pm 1.3$	51.3 ± 2.3
$N_2/N_{\mathrm{one\text{-}side}}$	$11.6 \pm 0.3 \pm 0.5$	12.7 ± 0.8	$11.94 \pm 0.03 \pm 0.56$	12.2 ± 0.8
$N_3/N_{\mathrm{one\text{-}side}}$	$3.6 \pm 0.2 \pm 0.2$	5.4 ± 0.7	$3.74 \pm 0.02 \pm 0.07$	5.4 ± 0.7
$N_4/N_{\mathrm{one\text{-}side}}$			$2.66 \pm 0.01 \pm 0.14$	3.7 ± 0.5

As seen from Table 5, similar fractions of 1n, 2n and 3n events are measured at $\sqrt{s_{\mathrm{NN}}} = 2.76$ TeV [5] and $\sqrt{s_{\mathrm{NN}}} = 5.02$ TeV. The dominance of 1n emission is evident at both collision energies. The measured 1n and 2n fractions are in very good agreement with RELDIS. A slight reduction of calculated 1n events is seen at higher energy because of the redistribution of events in favour of higher multiplicities. This can be explained by a higher average equivalent photon energy at $\sqrt{s_{\mathrm{NN}}} = 5.02$ TeV. However, such a subtle effect cannot be traced with confidence because of measurement and modelling uncertainties, which were calculated as described in Section 4.3.

5.3 Emission of neutrons without protons

In order to measure the cross section for 1n, 2n, ... 5n emission without proton emission (0p), the energy spectra in ZNC and ZNA were obtained for events not having a signal in the respective ZP. Measured cross sections of 1n-, 2n-, 3n-, 4n- and 5n-emission without protons are given in Table 6 together with

Table 6: Cross sections of emission of one, two, three, four and five neutrons without protons on the same side in the EMD of ^{208}Pb at $\sqrt{s_{NN}} = 5.02$ TeV, measured on the C and A sides, and their average along with their statistical and systematic uncertainties. Cross sections calculated with RELDIS are given for comparison. The sum of 1n–5n cross sections is presented in the last row. The uncertainties of the measurements are given in the order $\pm$ (stat.) $\pm$ (syst.).

ZN	ZP	$\sigma(in, 0p)$ (b)		$\sigma(in, 0p)$ (b)	$\sigma^{RELDIS}(in, 0p)$ (b)
		Side C	Side A		
1n		$92.6 \pm 0.1 \pm 3.8$	$90.9 \pm 0.1 \pm 3.9$	$91.8 \pm 0.1 \pm 3.3$	104.1 ± 5.2
2n		$21.4 \pm 0.1 \pm 0.8$	$20.0 \pm 0.1 \pm 2.0$	$20.7 \pm 0.1 \pm 1.1$	21.9 ± 1.1
3n	0p	$6.14 \pm 0.07 \pm 0.27$	$6.21 \pm 0.04 \pm 0.23$	$6.17 \pm 0.04 \pm 0.20$	7.59 ± 0.38
4n		$4.21 \pm 0.04 \pm 0.23$	$4.08 \pm 0.04 \pm 0.42$	$4.15 \pm 0.03 \pm 0.25$	4.29 ± 0.22
5n		$3.16 \pm 0.04 \pm 0.47$	$3.08 \pm 0.03 \pm 0.36$	$3.12 \pm 0.03 \pm 0.30$	2.95 ± 0.15
1n–5n				$126.0 \pm 0.2 \pm 4.0$	140.8 ± 5.3

RELDIS results. As can be seen, the cross sections measured on side C are systematically slightly larger than on side A, but the difference remains within the uncorrelated uncertainty of side A cross sections for all neutron multiplicities. The cross sections were calculated with Eq. (3) from the numbers of events n_i of each neutron multiplicity in obtained from the fit of spectra with the functions given by Eq. (1). In this case of 0p measurements, the numbers of true events of each multiplicity N_i were obtained by correcting for the efficiency of ZNC and ZNA and also for protons undetected in ZPC and ZPA, as described in Section 4.2. Statistical and systematic uncertainties were calculated as described in Sections 4.3 and 5.1. Contributions to the total systematic uncertainties are presented in Table 3.
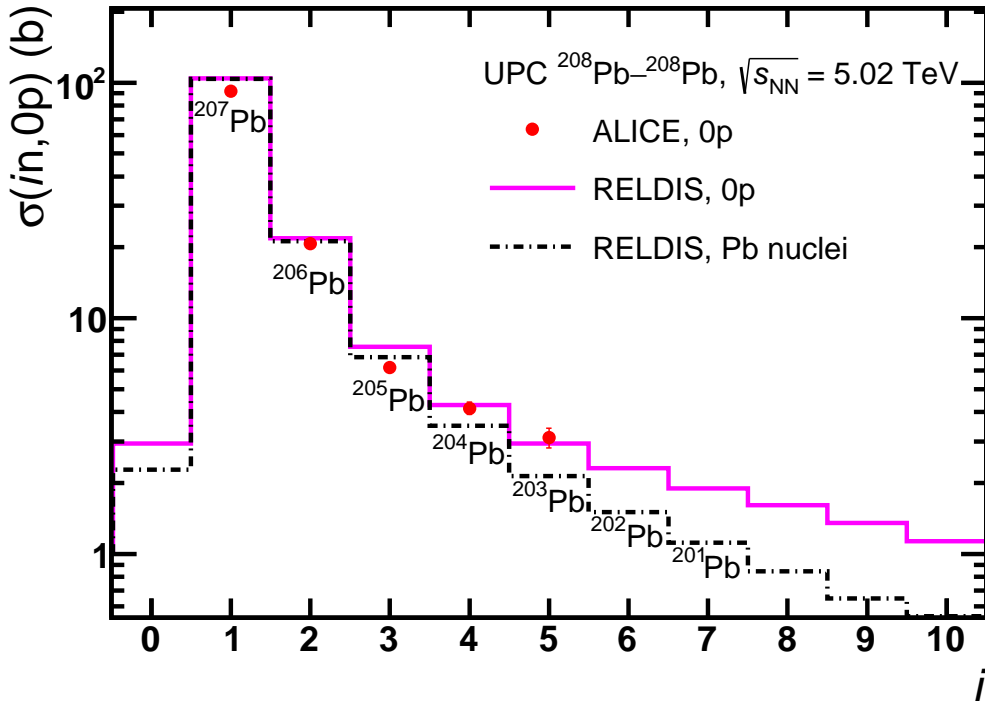
The measured cross sections of 1n, 2n, ... 5n emission not accompanied by protons, shown in Table 6, are lower than the cross sections of 1n, 2n,.. 5n emission along with other particles presented in Table 4. This difference is larger for 4n and 5n channels because protons are emitted more frequently at higher equivalent photon energies associated with multineutron events. With the exception of 5n emission, the measured 0p cross sections are lower than the cross sections calculated with RELDIS. Nevertheless, the agreement between the measurements and calculations for 0p cross sections is better than for Yp cross sections presented in Table 4.

The sum of the measured 0p cross sections from 1n to 5n is estimated as $126.0 \pm 0.2 \pm 4.0$ b. It is also listed in Table 6 for comparison with RELDIS. This sum of 0p cross sections provides a dominant ($\sim 83\%$) contribution to the sum of Yp cross sections $151.5 \pm 0.2 \pm 4.6$ b given in Table 4. In other words, only $\sim 17\%$ of 1n–5n events are accompanied by the emission of protons.

The measured 0p neutron emission cross sections are shown in Fig. 3 and compared with RELDIS results for the same cross sections and also with the calculated cross sections to produce specific secondary nuclei: ^{207,206,205,204,203}Pb. According to RELDIS, the cross section of the production of ^{207}Pb, is almost the same as (1n,0p) cross section, while the cross sections of production of ^{206}Pb and ^{205}Pb are smaller than (2n,0p) and (3n,0p) cross sections only by 3% and 10%, respectively. According to this model, the calculated 0p cross sections of emission of four, five, six and seven neutrons can be considered as upper limits for the cross sections of production of ^{204,203,202,201}Pb, respectively. The difference is due to the emission of additional particles, e.g. protons and/or charged π-mesons, which leave residual nuclei other than Pb, as explained in Section 6.

6 Discussion

The measured cross sections $\sigma(in)$ of neutron emission accompanied by an arbitrary number of protons in EMD can be used to validate various EMD models. The cross sections of neutron emission $\sigma(in, 0p)$

Figure 3: Colour online: measured cross sections of emission of given numbers of neutrons i in UPCs of ^{208}Pb nuclei at $\sqrt{s_{NN}} = 5.02$ TeV without proton emission (points) and the cross sections calculated with RELDIS [4] (solid-line histogram). Calculated cross sections to produce specific secondary nuclei, ^{207,206,205,204,203,202,201}Pb, are presented by the dash-dotted histogram marked by nuclide symbols. Combined statistical and systematic uncertainties of the measurements are presented.

without protons were also measured. Because of the absence of proton emission, these cross sections can be associated with the production of ^{207}Pb, ^{206}Pb, ^{205}Pb, ^{204}Pb and ^{203}Pb as secondary nuclei in EMD of ^{208}Pb.

In order to test this association, the RELDIS event generator, validated with data on neutron emission [5, 32] and production of secondary nuclei [3] in EMD of ^{208}Pb at lower collision energies, was used. In each simulated event $\Delta A = A_{res} + N_n + N_p - 208$ and $\Delta Z = Z_{res} + N_p - 82$ were calculated from the mass number A_{res} and charge Z_{res} of the heaviest residual nucleus and the numbers of emitted neutrons N_n and protons N_p. The calculated probability distributions to obtain ΔA and ΔZ in events with a given N_n are presented in Fig. 4. As seen from this figure, in RELDIS simulations the probabilities to obtain 1n, 2n, ... 5n events with $\Delta A = 0$ or $\Delta Z = 0$ among all EMD events are within the range of 3–50%. However, the probability of 1n, 2n, ... 5n events with $\Delta A < 0$ or $|\Delta Z| > 0$ is well below 1%.

Two examples of such rare events are presented in the following. The first one is represented by the excitation of an intranuclear neutron with its conversion to a proton: $\gamma n \rightarrow \Delta^o \rightarrow p + \pi^-$. In the case of the undetected π^- escaping the nucleus, the total charge of the system, including emitted nucleons, differs from 82: $\Delta Z = 1$. In Ref. [36] the production of $_{83}$Bi from 158A GeV $_{82}$Pb nuclei in their ultraperipheral collisions with different targets has been explained by the production of π^-. In the second example, the products of the fragmentation contain an undetected α-particle in addition to nucleons: $\Delta A = -4$. In Ref. [37] a similar reaction of the emission of α-particles from ^{197}Au induced by bremsstrahlung photons was investigated.

One can conclude from Fig. 4 that, according to RELDIS, in the majority of 1n–5n EMD events $\Delta A = 0$ and $\Delta Z = 0$, and it is sufficient to measure N_n and N_p for evaluating A_{res} and Z_{res}. The dominance of
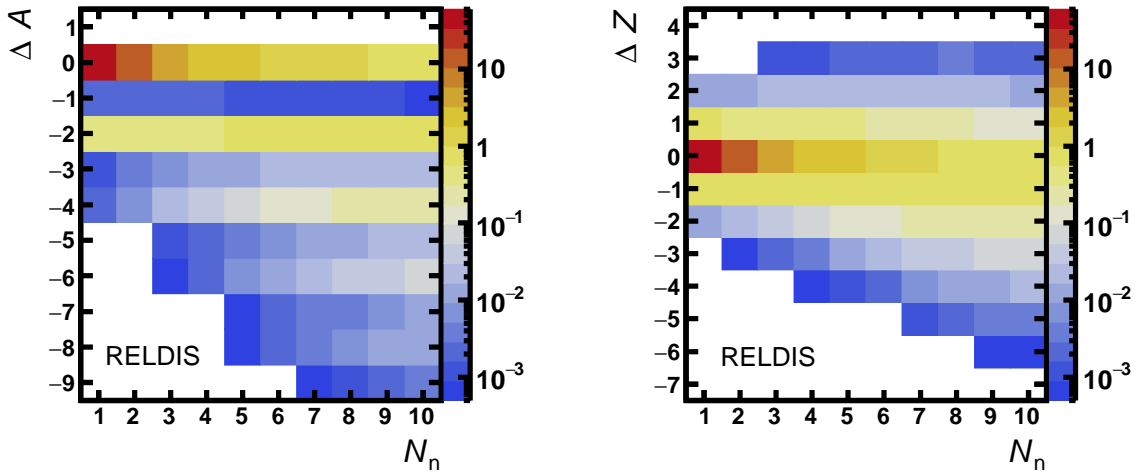
Figure 4: Colour online: Probability, calculated with RELDIS (in %), of the difference ΔA between the sum of the mass number of the most heavy residual nucleus and the numbers of emitted nucleons and A of the initial ^{208}Pb (left) and probability (in %) of the difference ΔZ between the sum of the charge of the most heavy residual nucleus and the number of emitted protons and Z of ^{208}Pb (right) plotted as functions of N_n in each event.

$\Delta A = 0$ and $\Delta Z = 0$ events is explained by a rather modest excitation energy per nucleon $E^\star/A$ delivered in the absorption of Weizsäcker–Williams photons by ^{208}Pb. This was demonstrated in Ref. [33] where $\langle E^\star/A \rangle$ were calculated for photospallation of ^{nat}Pb by real photons with energies from 20 MeV to 4 GeV. As found in Ref. [33], $\langle E^\star/A \rangle$ is typically below 1 MeV. This suggests the creation of an excited single heavy nuclear residue as a result of the emission of free neutrons and protons during the intranuclear cascade. Such an excited nucleus would evaporate few nucleons and possibly undergo nuclear fission [33] rather than a multi-fragment break-up which becomes possible only at $E^\star/A > 3$ MeV [38]. For example, the decay of the giant dipole resonance in ^{208}Pb with $E^\star = 7$–20 MeV mostly produces one neutron [39]. According to RELDIS [20], the production of two neutrons is ten times less frequent in EMD of ^{208}Pb in this interval of $E^\star$. The residual nuclei, ^{207}Pb or ^{206}Pb, can be distinguished by detecting the number of emitted neutrons.

The contribution of electromagnetically induced fission of ^{208}Pb in UPCs can also be estimated with RELDIS. The fission process violates the condition $\Delta A = 0$ and $\Delta Z = 0$, but its calculated probability at $\sqrt{s_{NN}} = 5.02$ TeV is as low as 0.6%. The EM fission probability for 158A GeV ^{208}Pb projectiles on Pb target is calculated with RELDIS as 0.18%. It is of the same order as the fission probabilities of 0.66% and 0.75% measured at the CERN SPS in Refs. [40] and [41], respectively. One can conclude that both theory and experiment indicate fission probabilities below 1%. This process can be safely neglected in favour of the creation of a single residual nucleus and several nucleons in EMD of ^{208}Pb.

7 Conclusions and outlook

The cross sections for emission of given numbers of forward neutrons in EMD of ^{208}Pb nuclei in ultraperipheral collisions at $\sqrt{s_{NN}} = 5.02$ TeV have been measured with the ALICE neutron zero degree calorimeters. The fractions of 1n, 2n and 3n events were measured at the highest ^{208}Pb–^{208}Pb collision energy available so far in accelerator experiments. These fractions were found to be similar to those measured at $\sqrt{s_{NN}} = 2.76$ TeV. The predictions from the RELDIS [4] and n$_O^O$n [23] models describe well the measured cross sections, in particular, for low neutron multiplicities. These measurements are important for the extraction of the contributions of high- and low-energy photons from coherent vector

meson photoproduction measurements accompanied by neutron emission [42, 43].

The cross sections of EMD events with the emission of exactly 1, 2, 3, 4 and 5 neutrons and without emission of protons have been measured. According to the RELDIS model, in EMD a single heavy residual nucleus is typically produced after the emission of several nucleons. The probability of nuclear fission in EMD is estimated to be below 1%. Therefore, the EMD events of 1n, 2n, 3n, 4n and 5n emission without protons can be associated with the production of ^{207}Pb, ^{206}Pb, ^{205}Pb, ^{204}Pb and ^{203}Pb, respectively. In other words, the measured neutron emission cross sections can be considered as upper limits for the respective isotope production cross sections.

Since the charge-to-mass ratio of ^{207}Pb remains close to ^{208}Pb, these frequently produced secondary nuclei emerge from the interaction points and propagate in the field of the LHC magnets on dispersive trajectories in the vicinity of the primary beam [7]. The collider collimation system is adjusted to intercept them (off-momentum collimators around Point 3 of LHC) to avoid the risk of beam dumps or quenches of superconducting magnets [7, 8, 44, 45]. The moderate fluxes of ^{206}Pb nuclei may hit the beam pipe closer to the interaction points. The smaller fluxes of $^{205,204,\cdots}$Pb generated in the collisions are lost at the start of the dispersion suppressor or taken up by physics debris absorbers and do not present any risks in collider operation.

A good quantitative understanding of the cross sections and fluxes of these nuclei provides valuable input for evaluating luminosity decay and beam losses in the design of the Future Circular Collider (FCC-hh) [46]. They also increase confidence in similar calculations for interactions of beam nuclei with carbon and other materials in the collimation systems of the LHC and FCC [8].

References

[1] G. Roland, K. Safarik, and P. Steinberg, "Heavy-ion collisions at the LHC",
Prog. Part. Nucl. Phys. **77** (2014) 70–127.

[2] **NA49** Collaboration, H. Appelshäuser *et al.*, "Spectator nucleons in Pb + Pb collisions at 158-A-GeV", *Eur. Phys. J. A* **2** (1998) 383–390.

[3] C. Scheidenberger *et al.*, "Charge-changing interactions of ultrarelativistic Pb nuclei",
Phys. Rev. C **70** (2004) 014902.

[4] I. A. Pshenichnov, "Electromagnetic excitation and fragmentation of ultrarelativistic nuclei",
Phys. Part. Nucl. **42** (2011) 215–250.

[5] **ALICE** Collaboration, B. Abelev *et al.*, "Measurement of the cross section for electromagnetic dissociation with neutron emission in Pb–Pb collisions at $\sqrt{s_{NN}} = 2.76$ TeV",
Phys. Rev. Lett. **109** (2012) 252302, arXiv:1203.2436 [nucl-ex].

[6] A. J. Baltz, M. J. Rhoades-Brown, and J. Weneser, "Heavy ion partial beam lifetimes due to Coulomb induced processes", *Phys. Rev. E* **54** (1996) 4233–4239.

[7] R. Bruce, D. Bocian, S. Gilardoni, and J. M. Jowett, "Beam losses from ultraperipheral nuclear collisions between ^{208}Pb^{82+} ions in the Large Hadron Collider and their alleviation",
Phys. Rev. ST Accel. Beams **12** (2009) 071002.

[8] P. D. Hermes, R. Bruce, J. M. Jowett, S. Redaelli, B. Salvachua Ferrando, G. Valentino, and D. Wollmann, "Measured and simulated heavy-ion beam loss patterns at the CERN Large Hadron Collider", *Nucl. Instrum. Meth. A* **819** (2016) 73–83.

[9] A. S. Botvina *et al.*, "Multifragmentation of spectators in relativistic heavy ion reactions",
Nucl. Phys. A **584** (1995) 737–756.

[10] A. Schüttauf *et al.*, "Universality of spectator fragmentation at relativistic bombarding energies", *Nucl. Phys. A* **607** (1996) 457–486, arXiv:nucl-ex/9606001.

[11] P. Deines-Jones *et al.*, "Charged particle production in the Pb + Pb system at 158 GeV/c per nucleon", *Phys. Rev. C* **62** (2000) 014903, arXiv:hep-ex/9912008.

[12] S. Cecchini, G. Giacomelli, M. Giorgini, G. Mandrioli, L. Patrizii, V. Popa, P. Serra, G. Sirri, and M. Spurio, "Fragmentation cross-sections of 158A GeV Pb ions in various targets measured with CR39 nuclear track detectors", *Nucl. Phys. A* **707** (2002) 513–524, arXiv:hep-ex/0201039.

[13] U. Uggerhøj, I. A. Pshenichnov, C. Scheidenberger, H. D. Hansen, H. Knudsen, E. Uggerhøj, P. Sona, A. Mangiarotti, and S. Ballestrero, "Charge-changing interactions of ultrarelativistic In nuclei", *Phys. Rev. C* **72** (2005) 057901.

[14] S. Tarafdar, Z. Citron, and A. Milov, "A Centrality Detector Concept", *Nucl. Instrum. Meth. A* **768** (2014) 170–178, arXiv:1405.4555 [nucl-ex].

[15] **AFP** Collaboration, S. Grinstein, "The ATLAS Forward Proton Detector (AFP)", *Nucl. Part. Phys. Proc.* **273-275** (2016) 1180–1184.

[16] G. Puddu *et al.*, "The zero degree calorimeters for the ALICE experiment", *Nucl. Instrum. Meth. Phys. Res. Sect. A* **581** (2007) 397–401.

[17] R. Gemme *et al.*, "Commissioning and calibration of the zero degree calorimeters for the ALICE experiment", *Nucl. Phys. B Proc. Suppl.* **197** (2009) 211–214.

[18] C. Oppedisano *et al.*, "Physics performance of the ALICE zero degree calorimeter", *Nucl. Phys. B Proc. Suppl.* **197** (2009) 206–210.

[19] I. A. Pshenichnov, I. N. Mishustin, J. P. Bondorf, A. S. Botvina, and A. S. Ilinov, "Particle emission following Coulomb excitation in ultrarelativistic heavy ion collisions", *Phys. Rev. C* **60** (1999) 044901, arXiv:nucl-th/9901061.

[20] I. A. Pshenichnov, J. P. Bondorf, I. N. Mishustin, A. Ventura, and S. Masetti, "Mutual heavy ion dissociation in peripheral collisions at ultrarelativistic energies", *Phys. Rev. C* **64** (2001) 024903, arXiv:nucl-th/0101035.

[21] H. H. Braun, A. Fassò, A. Ferrari, J. M. Jowett, P. R. Sala, and G. I. Smirnov, "Hadronic and electromagnetic fragmentation of ultrarelativistic heavy ions at LHC", *Phys. Rev. ST Accel. Beams* **17** (2014) 021006.

[22] M. Klusek-Gawenda, M. Ciemala, W. Schafer, and A. Szczurek, "Electromagnetic excitation of nuclei and neutron evaporation in ultrarelativistic ultraperipheral heavy ion collisions", *Phys. Rev. C* **89** (2014) 054907, arXiv:1311.1938 [nucl-th].

[23] M. Broz, J. G. Contreras, and J. D. Tapia Takaki, "A generator of forward neutrons for ultra-peripheral collisions: n_O^On", *Comput. Phys. Commun.* **253** (2020) 107181, arXiv:1908.08263 [nucl-th].

[24] **ALICE** Collaboration, K. Aamodt *et al.*, "The ALICE experiment at the CERN LHC", *JINST* **3** (2008) S08002.

[25] S. van der Meer, "Calibration of the effective beam height in the ISR", tech. rep., CERN, Geneva, 1968. https://cds.cern.ch/record/296752.

[26] **ALICE** Collaboration, S. Acharya, D. Adamová, A. Adler, J. Adolfsson, *et al.*, "ALICE luminosity determination for Pb−Pb collisions at $\sqrt{s_{NN}} = 5.02$ TeV", `arXiv:2204.10148 [nucl-ex]`.

[27] A. O. Svetlichnyi and I. A. Pshenichnov, "Formation of Free and Bound Spectator Nucleons in Hadronic Interactions between Relativistic Nuclei", *Bull. Russ. Acad. Sci. Phys.* **84** (2020) 911–916.

[28] T. Ullrich and Z. Xu, "Treatment of errors in efficiency calculations", 2007. `https://arxiv.org/abs/physics/0701199`.

[29] A. J. Baltz, Y. Gorbunov, S. R. Klein, and J. Nystrand, "Two-photon interactions with nuclear breakup in relativistic heavy ion collisions", *Phys. Rev. C* **80** (2009) 044902, `arXiv:0907.1214 [nucl-ex]`.

[30] S. R. Klein, J. Nystrand, J. Seger, Y. Gorbunov, and J. Butterworth, "STARlight: A Monte Carlo simulation program for ultra-peripheral collisions of relativistic ions", *Comput. Phys. Commun.* **212** (2017) 258–268, `arXiv:1607.03838 [hep-ph]`.

[31] U. Dmitrieva and I. Pshenichnov, "On the performance of Zero Degree Calorimeters in detecting multinucleon events", *Nucl. Instrum. Meth. A* **906** (2018) 114–119, `arXiv:1805.01792 [physics.ins-det]`.

[32] M. B. Golubeva *et al.*, "Neutron emission in electromagnetic dissociation of ultrarelativistic Pb ions", *Phys. Rev. C* **71** (2005) 024905.

[33] I. A. Pshenichnov, B. L. Berman, W. J. Briscoe, C. Cetina, G. Feldman, P. Heimberg, A. S. Iljinov, and I. I. Strakovsky, "Intranuclear-cascade model calculation of photofission probabilities for actinide nuclei", *Eur. Phys. J. A* **24** (2005) 69–84, `arXiv:nucl-th/0303070`.

[34] I. A. Pshenichnov and S. A. Gunin, "Electromagnetic interactions of nuclei at the FCC-hh collider", *Phys. Part. Nucl.* **50** (2019) 501–505.

[35] V. Muccifora *et al.*, "Photoabsorption on nuclei in the shadowing threshold region", *Phys. Rev. C* **60** (1999) 064616, `arXiv:nucl-ex/9810015`.

[36] C. Scheidenberger *et al.*, "Electromagnetically induced nuclear-charge pickup observed in ultrarelativistic Pb collisions", *Phys. Rev. Lett.* **88** (2002) 042301.

[37] J. O. Adler, G. Andersson, and H. A. Gustafsson, "Alpha particles from ^{197}Au irradiated by 500 MeV bremsstrahlung", *Nucl. Phys. A* **223** (1974) 145–156.

[38] J. P. Bondorf, A. S. Botvina, A. S. Ilinov, I. N. Mishustin, and K. Sneppen, "Statistical multifragmentation of nuclei", *Phys. Rept.* **257** (1995) 133–221.

[39] V. V. Varlamov, A. I. Davydov, and V. N. Orlin, "New evaluated data on ^{206,207,208}Pb photodisintegration", *Eur. Phys. J. A* **57** (2021) 287.

[40] B. Alessandro *et al.*, "Fission cross sections of lead projectiles in Pb nucleus interactions at 40 and 158 GeV/c per nucleon", *Phys. Rev. C* **69** (2004) 034904.

[41] **NA50** Collaboration, M. C. Abreu *et al.*, "Observation of fission in Pb–Pb interactions at 158A GeV", *Phys. Rev. C* **59** (1999) 876–883.

[42] V. Guzey, M. Strikman, and M. Zhalov, "Disentangling coherent and incoherent quasielastic J/ψ photoproduction on nuclei by neutron tagging in ultraperipheral ion collisions at the LHC", *Eur. Phys. J. C* **74** (2014) 2942, `arXiv:1312.6486 [hep-ph]`.

[43] Z. Citron *et al.*, "Report from Working Group 5: Future physics opportunities for high-density QCD at the LHC with heavy-ion and proton beams", *CERN Yellow Rep. Monogr.* **7** (2019) 1159–1410, `arXiv:1812.06772 [hep-ph]`.

[44] S. R. Klein, "Localized beam pipe heating due to e$^-$ capture and nuclear excitation in heavy ion colliders", *Nucl. Instrum. Meth. A* **459** (2001) 51–57, `arXiv:physics/0005032`.

[45] M. Schaumann, J. M. Jowett, C. Bahamonde Castro, R. Bruce, A. Lechner, and T. Mertens, "Bound-free pair production from nuclear collisions and the steady-state quench limit of the main dipole magnets of the CERN Large Hadron Collider", *Phys. Rev. Accel. Beams* **23** (2020) 121003, `arXiv:2008.05312 [physics.acc-ph]`.

[46] M. Schaumann, "Potential performance for Pb-Pb, p-Pb and p-p collisions in a future circular collider", *Phys. Rev. ST Accel. Beams* **18** (2015) 091002, `arXiv:1503.09107 [physics.acc-ph]`.